Atomization and Sprays, 23 (7): 623–641 (2013)

ANALYZING THE CYCLE-TO-CYCLE VARIATIONS OF PULSING SPRAY CHARACTERISTICS BY MEANS OF THE PROPER ORTHOGONAL DECOMPOSITION

Hao Chen,[1] David L. S. Hung,[1,2,*] Min Xu,[1] & Jie Zhong[2]

[1] *School of Mechanical Engineering, Shanghai Jiao Tong University, National Engineering Laboratory for Automotive Electronic Control Technology, Shanghai 200240, China*

[2] *University of Michigan-Shanghai Jiao Tong University Joint Institute, Shanghai Jiao Tong University, Shanghai 200240, China*

[*] Address all correspondence to David L. S. Hung E-mail: dhung@sjtu.edu.cn

Original Manuscript Submitted: 05/17/2013; Final Draft Received: 07/02/2013

This paper presents a novel approach to analyze the cycle-to-cycle variations of pulsing spray characteristics. The purpose is to quantify the cycle-to-cycle variations of the macroscopic characteristics of spark-ignition direct-injection (SIDI) fuel injector spray, so that improvements of air-fuel mixture formation can be made to enhance the combustion efficiency and reduce emissions of SIDI engines. The experiments were carried out using an eight-hole SIDI fuel injector under a controlled ambient environment with an extended range of test conditions. Using a strobe light as an illumination source, multiple cycles of macroscopic spray structure images at a fixed injection delay time were taken by a CCD camera. The proper orthogonal decomposition (POD) technique was implemented to analyze the cycle-to-cycle characteristics of spray variation. In addition, the effects of injection pressure, ambient pressure, and fuel type on spray variation were also investigated. POD analysis reveals that the mode 1 pattern captured the ensemble-averaged spray shape, the mode 2 pattern provided quantification of spatial fuel distribution variations of different cycles of spray, and higher mode patterns further quantified the finer details of the variations surrounding the well-atomized periphery of the spray structure. POD analysis also quantitatively confirms that better-atomized sprays led to slightly higher variations of finer structures along the spray boundary. Overall, this study demonstrates that POD analysis can be used as a novel approach to quantify the cycle-to-cycle variation of pulsing spray characteristics.

KEY WORDS: *cycle-to-cycle variation, pulsing spray characteristics, proper orthogonal decomposition*

1. INTRODUCTION

To enhance the fuel economy and reduce pollutant emissions, spark-ignition direct-injection (SIDI) engines have gained popularity in modern vehicles (Zhao et al., 1999). In SIDI engines, fuel is directly injected into the combustion chamber. Thus, a high-quality air-fuel mixture is required for successful combustion in broad engine load and speed ranges (Aleiferis et al., 2010; Zeng et al., 2012a, 2013). However, strong cycle-to-cycle variations in the air-fuel mixture increase the coefficient of variation (COV) of indicated mean effective pressure (IMEP), thereby leading to combustion instabilities that result in increased fuel consumption, hydrocarbon (HC) emission, and poor drivability (Ozdor et al., 1994).

The optimization of fuel spray structure in a SIDI combustion system is a crucial step for the SIDI engine development (Elbadawy et al., 2011; Kay et al., 2012; Zhang et al., 2012a,b). For a homogeneous-charge SIDI engine, the fuel is injected into the cylinder during the intake stroke. Therefore, the goal is (i) to acquire an optimum fuel-air mixture uniformity at the time of ignition, and (ii) to avoid or at least minimize the spray impingement on the piston top and cylinder liner (Hung et al., 2007). Because the fuel impingement on the engine cylinder dilutes the engine lubrication, fuel splashing on the piston would lead to a pool fire and increase the unburned HC emission. For the stratified-charge lean-burn SIDI engine, fuel is injected late during the compression stroke. Therefore, in addition to the goals aforementioned, another important objective is to create an ignitable mixture near the spark plug and leave the periphery region of the combustion chamber with a lean mixture for the specific range of engine speed and load. As a result, large cycle-to-cycle variations of fuel spray have been observed and, for some cycles, the fuel spray plume cannot meet these requirements. For the extreme case, spray variation at stratified-charge SIDI mode could lead to misfire due to the very limited fuel-air mixture formation time between the fuel injection and spark timing.

Researchers have developed different techniques to study the cycle-to-cycle variation of fuel spray (Hung et al., 2003; Zhong et al., 2012). Hung et al. (2003) presented the presence probability image (PPI) technique to quantify the pulse-to-pulse variation of macroscopic fuel spray geometry for SIDI engine applications. More recently, Hung and Zhong (2011) studied the start of fuel cycle-to-cycle variation of solenoid-actuated high-pressure fuel injectors designed for SIDI engines using PPI. Their results demonstrated that a large degree of cyclic variation existed when the time delay after start of injection (SOI) was closer to its time of the opening response. Marchi et al. (2010) assessed the spray stability of the injector by analyzing the mean and root mean square (rms) images of the fuel spray. Their results revealed that the positive-step inward seal band design injector produced the most repeatable spray among their three prototype SIDI injectors. However, the PPI technique only provides information about the liquid spray presence probability and ignores the amount of fuel presence in a certain location. In addition,

using mean and rms images to analyze the spray variation could be misleading, because it is never certain the observed image is present in every cycle or only from certain dominant cycles.

In recent years, advanced optical diagnostic techniques have enabled high–frame rate imaging for hundreds of engine cycles (Sick et al., 2010; Sick, 2013). Meanwhile, large eddy simulation (LES) has been intensively explored to simulate the in-cylinder processes for multiple cycles (Haworth 1999, Enaux et al. 2011). Both methods create large amounts of data that are capable of revealing the cyclic variability. Thus, a powerful and elegant analysis tool for extracting useful information from the complicated data set is highly required. The proper orthogonal decomposition (POD) technique is proposed to fulfill this need. Over the past decade, POD has gained widespread use in engine research. First, POD is conventionally used to extract an optimal set of dominant (in terms of kinetic energy) spatial modes, so that only a small number of modes is needed to represent a particular engine flow condition, and the cycle-to-cycle variation of the flow can be described (Cosadia et al., 2006; Voisine et al. 2011). Second, POD has been employed for low-order modeling of flows [i.e., reconstructing the principal flow dynamics with the least number of modes (Fogleman et al., 2004)]. Third, POD has been implemented to recover the time information between two sequential PIV time measurements (Druault et al., 2005). Fourth, POD has been used to provide a platform for quantitative comparison between different data sets. Therefore, the cyclic-varied LES data can be validated by the cycle-to-cycle PIV data (Sick et al., 2011). Also, Chen et al. (2011) quantitatively compared the flow fields and the equivalence ratio distributions at spark timing from well-burning and misfiring cycles so that the reasons for misfiring cycles could be identified. While the application of POD in engine flows is complicated and ambiguous, a practical guide on how to use and interpret POD in engine flows can be found in the literature (Chen et al., 2012, 2013). However, applying POD on the spray variation research has not been explored yet.

In the current work, POD analysis for spray variation is proposed and developed. The Mie scattering spray images of a multihole SIDI injector were recorded under two fuel injection pressures (5 and 10 MPa), three levels of ambient pressure (50, 100, and 500 kPa absolute pressure), and with three different fuels (n-heptane, gasoline, and ethanol) in a constant-volume chamber. The effects of the above parameters on the spray cycle-to-cycle variation were investigated using the POD method.

2. EXPERIMENTAL SETUP AND TEST PROCEDURE

Figure 1 depicts the schematic of the experimental setup. It consisted of a fuel supply system, a fuel temperature control system, a constant-volume chamber, a chamber pressurization system, a vacuum pumping system, and an imaging system. A piston accumulator with a pressurized nitrogen supply system was used to provide the required fuel injection pressure. The fuel temperature was adjusted by varying the temperature of

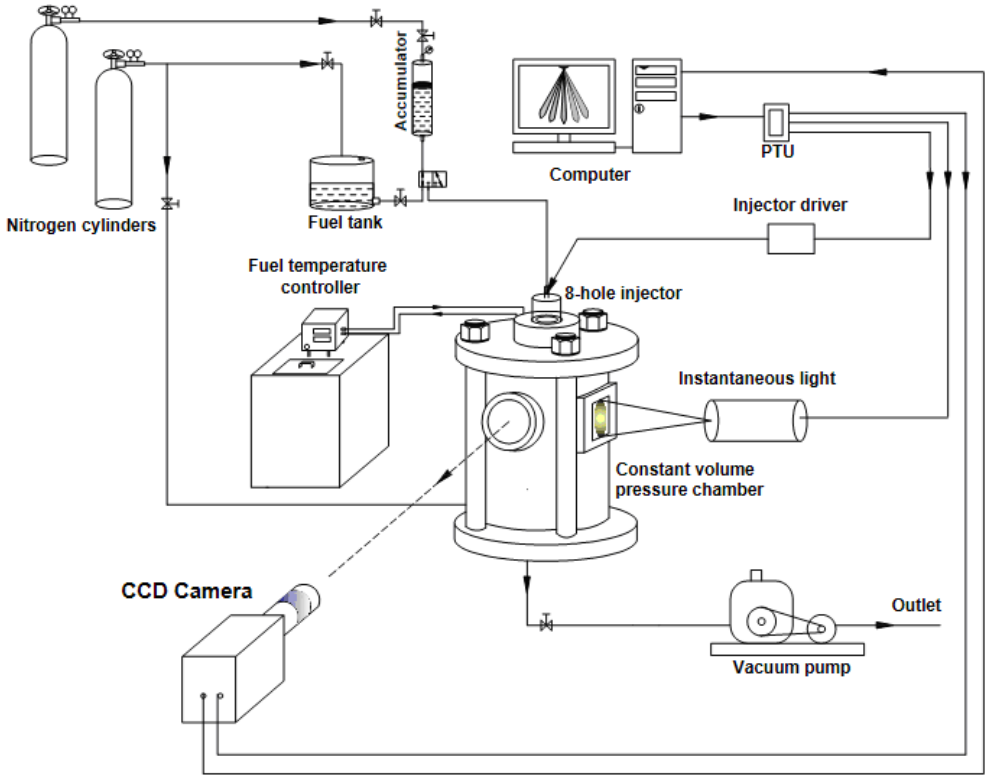

FIG. 1: Experimental setup.

water running through a water path surrounding the housing of the injector. The ambient pressure down to 20 kPa (absolute) was achieved through a vacuum pump, and up to 2 MPa by the supply of pressurized nitrogen. An eight-hole SIDI fuel injector was mounted vertically at the top of the constant-volume chamber. Four quartz windows surrounding the chamber provided full optical access to the fuel spray visualization inside the chamber. A strobe light was used to illuminate the fuel spray. Spray images were captured by the LaVision imaging system, which consisted of a CCD camera (LaVision Image Intense) and Nikon lens (f = 105 mm, $f\#$ = 4.5), which were positioned at an angle of 150 deg from the light source. A programmable timing unit (LaVision, PTU) was used to synchronize the strobe light and the CCD camera with the fuel injection timing. The post-processing of the acquired spray images was processed using the software DaVis 8.1 (LaVision). In addition, a compact code developed using MATLAB (2009b) was used for POD analysis of the spray. The MATLAB code and related documentation can be found in a previous paper (Chen et al., 2013).

Table 1 tabulates the experimental conditions. The ambient temperature was fixed at 25$\pm$1°C. The test fuels, namely, n-heptane, ethanol, and gasoline, were chosen and their physical properties are shown in Table 2. For each test condition of Table 1, a series

TABLE 1: Experimental conditions

Parameter	Value
Test fuels	n-heptane, ethanol, gasoline
Ambient temperature	25±1°C
Injection duration	1000 μs
Ambient pressure (absolute)	50, 100, 500 kPa
Fuel temperature	25°C
Injection pressure	5, 10 MPa

TABLE 2: Physical properties of the test fuels

25°C	n-heptane	Ethanol	Gasoline
Liquid viscosity (mPa·s)	0.38	1.05	0.42
Liquid density (kg/m^3)	679	783	740
Surface tension (mN/m)	16.3	22.5	22.1

of spray images as well as background images were recorded. The background image was subtracted from the spray image during image processing. Fifty images were taken at 1.3 ms after the start of injection (ASOI). This imaging condition was selected to illustrate a well-developed spray structure.

3. OVERVIEW OF PROPER ORTHOGONAL DECOMPOSITION

The starting point for POD analysis is to prepare a set of snapshot spray images for K different cycles ($S^{(k)}$, k = 1, 2, ..., K) as input images. Each snapshot image has the dimension of $I \times J$ pixels intensity distribution. Conceptually, the POD performs a linear decomposition of this given collection of input images, and creates M orthonormal spatial basis functions (POD modes φ_m, m = 1, 2, ..., M) and corresponding coefficients $c_m^{(k)}$

$$S^{(k)} = \sum_{m=1}^{M} c_m^{(k)} \varphi_m \tag{1}$$

where φ_m are scalar distributions with the same dimension ($I \times J$ pixels) as the input image. The number of input spray image (K) and POD modes number (M) are equal. If all M POD modes are used in Eq. (1), the exact input image can be reconstructed, and the lower-order estimation is obtained with a truncated POD mode set. More importantly, the POD modes are computed in the manner that the approximation for each m is as good [the actual interpretation is shown by Eq. (2)] as possible in the least square sense. In other words, a sequence of φ_m can be found so that the first two modes give the best possible two-term approximation, and the first 10 modes give the best possible 10-term approximation, and so on.

Therefore, mathematically, the objective of POD is to find a sequence of basis functions φ_m, which represents the dominant structures from a given scalar fields set. In this way, the following function is minimized:

$$\sum_{k=1}^{K} \left\| S^{(k)} - \sum_{m=1}^{M'} c_m^{(k)} \varphi_m \right\|^2 \tag{2}$$

The algorithm to achieve this minimization is shown as follows. The intensity for every pixel in the image is to be reordered into a row and put into the following matrix:

$$S = \begin{bmatrix} S^{(1)} \\ S^{(2)} \\ \vdots \\ S^{(K)} \end{bmatrix} = \begin{bmatrix} S^{(1)}_{i=1,j=1} & S^{(1)}_{i=1,j=2} & \cdots & S^{(1)}_{i=1,j=J} & S^{(1)}_{i=2,j=1} & \cdots & S^{(1)}_{i=I,j=J} \\ S^{(2)}_{i=1,j=1} & S^{(2)}_{i=1,j=2} & \cdots & S^{(2)}_{i=1,j=J} & S^{(2)}_{i=2,j=1} & \cdots & S^{(2)}_{i=I,j=J} \\ \cdots & \cdots & \cdots & \cdots & \cdots & \cdots & \cdots \\ S^{(K)}_{i=1,j=1} & S^{(K)}_{i=1,j=2} & \cdots & S^{(K)}_{i=1,j=J} & S^{(K)}_{i=2,j=1} & \cdots & S^{(K)}_{i=I,j=J} \end{bmatrix} \tag{3}$$

Then, the spatial matrix for the input images can be defined as

$$C = \frac{1}{K} S S^T \tag{4}$$

The minimization [Eq. (2)] is achieved by solving the eigenvalue problem of spatial correlation matrix C, such that

$$C\beta_m = \lambda_m \beta_m \tag{5}$$

The eigenvectors (β_m, m = 1, 2, ..., M) are ordered with the decreasing order of corresponding eigenvalues (λ_m, m = 1, 2, ..., M). This arrangement is important so only the first several POD modes can capture the majority of the total image intensity. The basis functions are calculated by projecting *S* onto the eigenvector β_m (m = 1, 2, ..., M), which are then normalized.

Finally, the coefficients of modes are computed by projecting the input spray images onto basis functions. Because the POD modes have been normalized, the coefficient $c_m^{(k)}$ contains the amplitude that the basis function, φ_m, contributes to the snapshot, $S^{(k)}$. The image intensity from all of the input images captured by the mth mode is

$$E_m = \sum_{k=1}^{K} \left(c_m^{(k)} \right)^2 \tag{6}$$

4. METRIC FOR QUANTITATIVE IMAGE PATTERN COMPARISON

When comparing the difference of a specific pattern between two images, it is useful to quantify the degree of similarity between them. Perhaps the most common approach is by direct visual comparison between the images to differentiate any observable variations among them. However, this approach normally requires thresholding the images,

which are semi-quantitative and heavily subjective to an individual's judgment. Hence, a nonsubjective metric to quantify the degree of which the image patterns of two images are similar or dissimilar is needed. In this study, the relevance index of two images, R_p, obtained by projecting one image $[S^{(1)}]$ on the other image $[S^{(2)}]$ is proposed to quantitatively compare the degree of similarity between two image patterns, as follows:

$$R_p = \left| \frac{S^{(1)}, S^{(2)}}{\left\| S^{(1)} \right\| \left\| S^{(2)} \right\|} \right| \tag{7}$$

The numerator is the inner product of pixel intensity of two images, and $||\cdot||$ denotes the L^2 norm. The R_p value varies from 0 to 1. R_p equals 1 if two images have the identical pattern. R_p = 0 if two image patterns are orthogonal (no similarity at all). Therefore, Fig. 2 illustrates how this relevance index is used. As displayed in Fig. 2, images 1 and 2 are selected from two different injectors, so their spray patterns are substantially different. Their relevance index is only 0.32. However, images 2 and 3 are created from the same image pattern, but they only differ in their pixel intensity (note that image 3 has been created by dividing the intensity of each pixel in image 2 by a factor of 2). Therefore, the relevance index between image 2 and image 3 is 1 because the two images contain the exact identical spray pattern. This illustrates one important feature of the relevance index, that is, R_p is a metric of the similarity of two image patterns without regard to the variation in the pixel intensity, which is not always obvious by direct visual comparison.

5. INTERPRETATION OF POD USING SYNTHETIC SCALAR FIELDS

In this section, the construction and the interpretation of POD modes are discussed with two illustrative examples. Simple synthetic 2D scalar fields (in this case, it is the spray pattern with different pixel intensity values) of snapshot spray images have been created

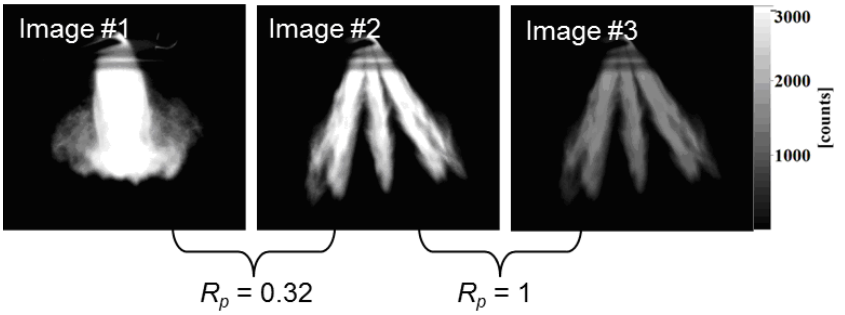

FIG. 2: The relevance index between sets of images. Images 1 and 2 have different spray patterns. Image 3 is obtained by dividing the intensity of each pixel in image 2 by a factor of two; therefore, images 2 and 3 have identical spray patterns.

to intuitively demonstrate the applicability of the POD for the quantification of spray variation over different injection pulses. It is worth mentioning that the illustration of the POD analysis is not only unique to the spray pattern, but also to other scalar field analyses where POD could be reasonably implemented.

5.1 Example 1: Using POD to Identify the Variation of Identical Spray Pattern with different Image Pixel Intensities

In the first illustrative example, three synthetic images of identical spray pattern are created, but the pixel intensity of the spray pattern has been scaled differently. Image 1 (12-bit image, with maximum intensity of 4095) depicts the base spray pattern with the maximum intensity of 1942 and the minimum value of 101. Outside the spray pattern is the area of the background with intensity randomly distributed over the spatial domain between 0 and 1. Images 2 and 3 are created in a similar manner, except that the spray pattern intensity of image 2 is 1.5 times that of image 1, and the spray pattern intensity of image 3 is two times that of the image 1. Therefore, all three images are composed of the identical spray pattern occupying the same pixel locations but with different pixel intensities.

Under this scenario, for the three synthetic images created, three POD modes and their coefficients can be constructed accordingly, as shown in Fig. 3. It is evident that the POD mode 1 (φ_1) fully captures the dominant spray pattern, which is almost identical to the ensemble-averaged image. As described in Section III, the modes are normalized so the sum of the square of the intensity over the mode pixels is equal to one. Physically, the modes only contain the spatial pattern of the spray and the intensity of the modes is captured by the POD coefficients. In this manner, the spatial pattern and its intensity are separated by the POD technique. For the three coefficients associated with mode 1,

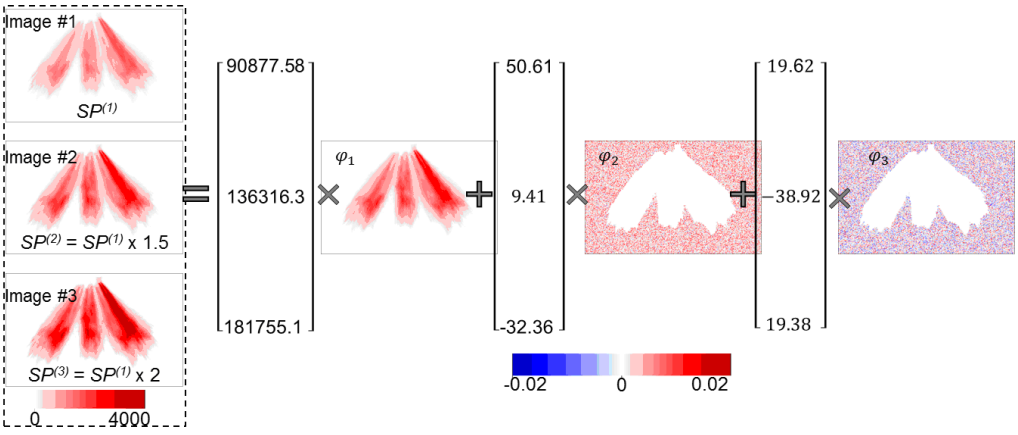

FIG. 3: Three synthetic scalar images (image 1, 2, 3) were decomposed into three POD modes and corresponding coefficients (SP: spray pattern).

the coefficient for image 2 is also 1.5 times as large as the coefficient for image 1, and the coefficient for image 3 is almost twice of that for image 1. This is reasonable since that spray pattern intensity in the original image 2 and image 3 is 1.5 times and two times, respectively, that of image 1. Therefore, the image intensity variation for the same spray pattern can be quantified by the POD coefficients. Because the first mode fully captures the dominant spray pattern, modes 2 and 3 only contain random background noise. Their coefficients are also much smaller compared to that of mode 1. This is because the background intensity is distributed randomly between 0 and 1, which is significantly smaller than the intensity of the pixels associated with the spray pattern in the image.

One may wonder why a negative value appears in mode 3. Considering the reconstruction of image 1 with all three modes and their associated coefficients, one can immediately realize that mode 1 and its coefficient resemble the dominant spray pattern. Moreover, modes 2 and 3 and their coefficients reconstruct the background noise. The sum of the contribution from all modes times their respective coefficients must equal the exact intensity value in image 1. Since mode 2 is generated taking into account all three images, the pixel intensity value might be larger than the intensity value in image 1 for certain pixels. Hence, this larger value requires summing a negative value to recreate the value at these pixels.

5.2 Example 2: Using POD to Quantify the Variation of Dissimilar Spray Patterns with different Image Pixel Intensities

The second example further illustrates how POD analysis is used to quantify the variation of dissimilar spray patterns. In this example, four spray patterns are synthesized to be the input images. Images 1, 2, and 3 contain the exact spray pattern, but the intensity of the spray pattern in images 2 and 3 is 1.5 and two times, respectively, that of image 1. The intensity outside of the spray pattern is again randomly assigned with the intensity value between 0 and 1 spatially. These three images are constructed in a similar manner as the ones in example 1. The difference is that the fourth image (image 4) contains a totally different spray pattern and with a similar background noise of intensity values between 0 and 1. Therefore, the four input images contain two distinct spray patterns and all with similar background noise intensity.

It is clear that the dominant spray pattern still resembles the first three images. However, with a different pattern existing in the midst of the dominant pattern, how will POD arrange the modes to capture, and more importantly to quantify, the variation in the spray pattern? The answer to this question is depicted graphically in Fig. 4. First, mode 1 still captures the dominant spray pattern as displayed in images 1, 2, and 3. The three large coefficients associated with mode 1 confirm their dominant pattern. Second, the much smaller coefficient associated with image 4 shows that mode 1 does not resemble the pattern as depicted in image 4.

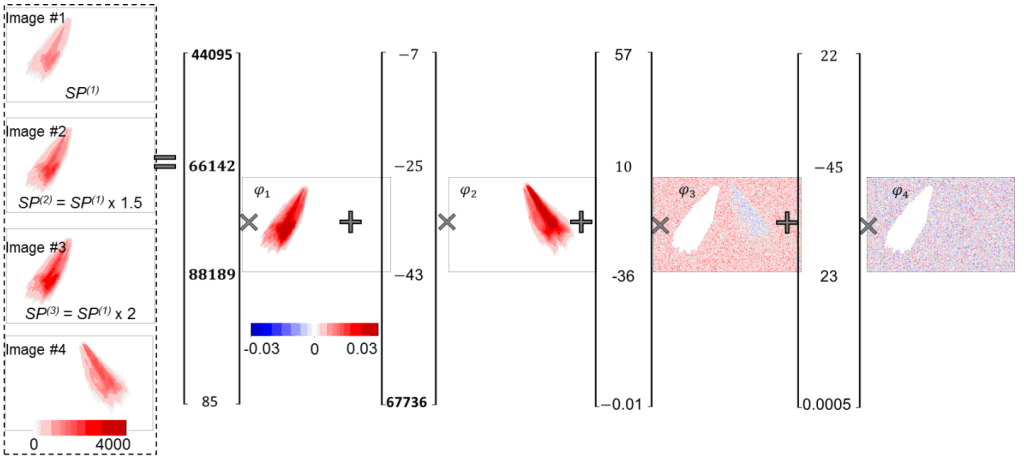

FIG. 4: Four synthetic scalar images (image 1, 2, 3, 4) were decomposed into four POD modes and corresponding coefficients (SP: spray pattern).

With regard to the different spray pattern of image 4, it is evident that mode 2 only captures the spray pattern resembled in image 4. The large coefficient associated with mode 2 for image 4 confirms the presence of mode 2 pattern in image 4. That is, the lower modes capture the dominant spray pattern (in terms of ensemble intensity for the particular pattern), and the higher modes only capture the relatively insignificant structures, such as the occasional appearance of the dissimilar spray pattern or the noise background (modes 3 and 4, as shown in Fig. 4). This demonstrates one important feature of POD analysis: image structure with identically repeated pattern and position are placed in one mode, and the sequence is arranged with decreasing order of ensemble intensity.

6. INTERPRETATION OF PUSLING SPRAY VARIATIONS USING POD ANALYSIS

The previous examples have provided some basic insight to interpret the pattern and coefficients of the POD modes. Compared to the synthetic scalar fields, the spray patterns of fuel injectors are far more complicated because they contain the superposition of multiple randomly distributed patterns with different spatial intensities and length scales. In the following section, the cycle-to-cycle variations of actual fuel spray images of n-heptane are illustrated using POD.

6.1 Interpretation of Spray Variation Using the Pattern and Coefficients of Mode 1

Figure 5 depicts the first POD mode (φ_1) computed from the 50 spray images. It is placed side by side with the ensemble-averaged image of the same 50 spray cycles.

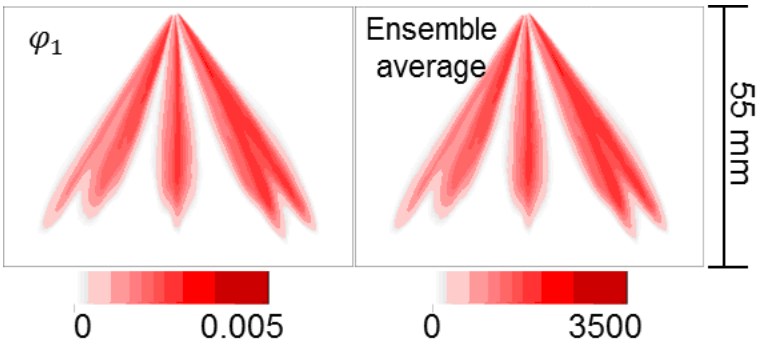

FIG. 5: Mode 1 and ensemble-averaged image comparison.

Even though the color bars below the images are of different physical quantities, the appearance of both patterns is almost identical. To quantitatively show the similarity degree of these two images, the relevance index R_p (already introduced in Section IV) is computed to be 0.99999987. The near unity of this R_p value confirms that mode 1 pattern is an excellent approximation of the ensemble-averaged image pattern. More importantly, mode 1 coefficients for all 50 cycles can be used to quantify the intensity variation of the spray cycles. This POD property has been clearly demonstrated in the previous examples of the synthetic scalar fields.

Figure 6 shows the comparison of mode 1 coefficients [Fig. 6(a)] with the total value of image intensity [Fig. 6(b)] for all 50 original spray images. These two curves show almost identical trends. In other words, the larger value of the mode 1 coefficient corresponds to the higher intensity of spray image. This illustrates that the mode 1 coefficients also capture the intensity variation of the original spray images from different cycles. Note that the image intensity is linked to the amount of liquid in the spray, since the higher intensity of spray image means that more fuel is present at the locations displayed in the mode 1 pattern.

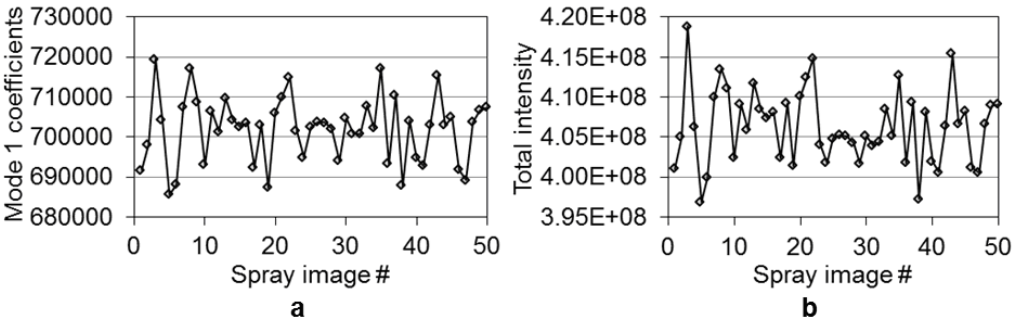

FIG. 6: (a) The mode 1 coefficients and (b) original spray image's total value of intensity for all 50 spray images.

6.2 Interpretation of Spray Variation Using the Pattern and Coefficients of Mode 2

The POD mode 2 pattern is associated with the spatial variations of the fuel distribution of different cycles. From a visual comparison of spray images, the fuel spray plumes of different cycles do not always appear at the exact same locations. The positions of the spray plumes vary slightly from cycle to cycle even though the differences are very subtle. A visual comparison of many cycles to quantify this variation would only be subjective and semiquantitative. However, the POD technique is best suited for capturing the variation of plume location.

Two individual spray cycles are used to further illustrate how the spatial difference of their distinct spray patterns can be quantified. For ease of discussion, only the variation of the center plume fuel distribution is elaborated. The POD mode 2 pattern and its coefficients distribution for all 50 spray images are depicted in Fig. 7. Cycle 7 is selected because the coefficient of mode 2 is negative. On the contrary, cycle 19 is chosen because the coefficient of mode 2 is positive. First, the center plume in the mode 2 pattern (Fig. 7) shows a clear separating line. The left part of the center plume has positive values while the right part is mostly composed of negative values. Therefore, multiplying the left part of the center plume with the positive mode 2 coefficients (such as that of cycle 19) would result in a higher value (in this case, this value represents the fuel amount) to the left side (red region in mode 2) of the center plume. This means that the spray is slightly displaced to the left side. Following through the same multiplication process, the negative mode 2 coefficient (such as that in cycle 7) would cause the center plume to be displaced slightly to the right side (blue region in mode 2). Overall, by combining the mode 2 pattern and its coefficient, the spatial variation of fuel distribution of the spray pattern from different spray cycles can be precisely captured and quantified.

To verify the above results from POD analysis, original spray images of cycles 7 and 19 (cycles identified by the POD coefficients in Fig. 7) and their spray boundary are overlapped, as shown in Fig. 8. It is clear that the center plume of cycle 7 is slightly displaced to the right side, and the center plume of cycle 19 shows minor displacement

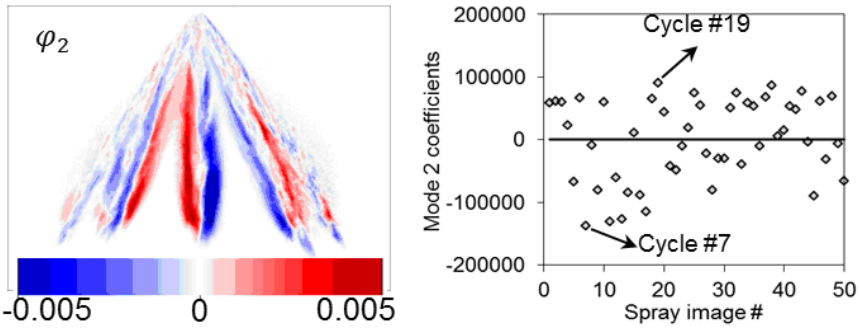

FIG. 7: POD mode 2 and its coefficients distribution for all 50 cycles.

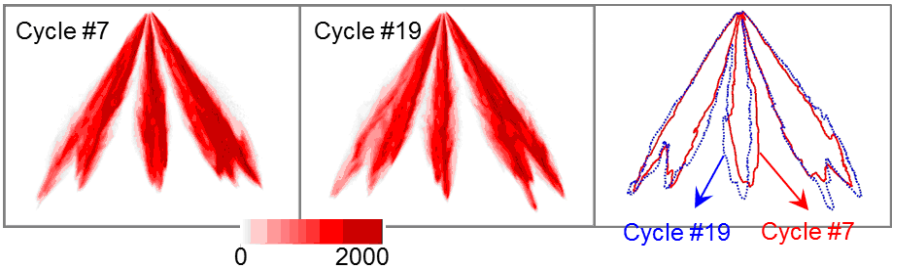

FIG. 8: Original spray images from specially selected cycles 7 and 19 (highlighted in Fig. 7)—their boundaries overlap.

to the left side. These results are consistent with the spatial variations of fuel distribution identified by the POD analysis method.

6.3 Interpretation of Spray Variation Using the Pattern and Coefficients of Higher Modes

The physical interpretations of higher modes are illustrated in this section. Figure 9 depicts three different mode patterns: they are modes 3, 10, and 50. It is clear that the spatial scales are becoming smaller as the mode number increases. In addition, the positive and negative spatial scales are distributed more randomly at higher modes. The reason is that the modes of POD are arranged in a decreasing sequence in terms of intensity. The larger spatial scale depicted in lower modes, such as mode 1, captures more intensity than the higher modes. Figure 10 shows the image intensity captured by all 50 modes. Mode 1 already captures 94.03% of the intensity fraction. It resembles the dominant ensemble-averaged spray pattern, which is a spatially large-scale structure. The higher modes, which only capture the small-scale patterns, contain much less intensity. For instance, mode 3, mode 10, and mode 50 capture 0.40, 0.18, and 0.03% of the intensity, respectively.

Figure 11 shows the original spray image of cycle 19 and its POD reconstructed mode patterns using the first mode, the first two modes, and all 50 modes. It is clear

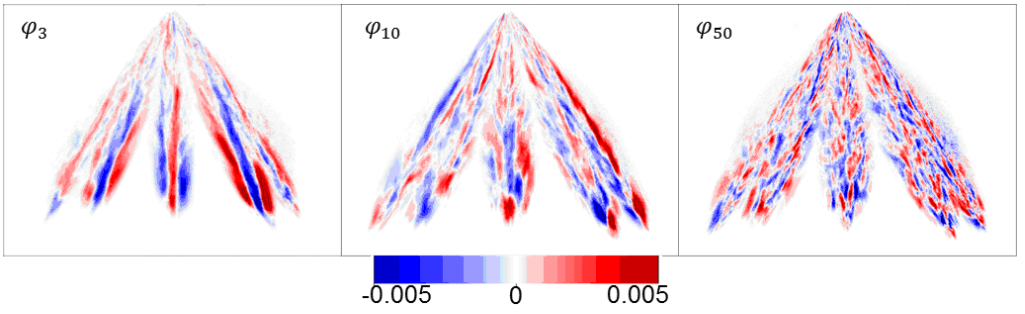

FIG. 9: POD mode 3, mode 10, and mode 50.

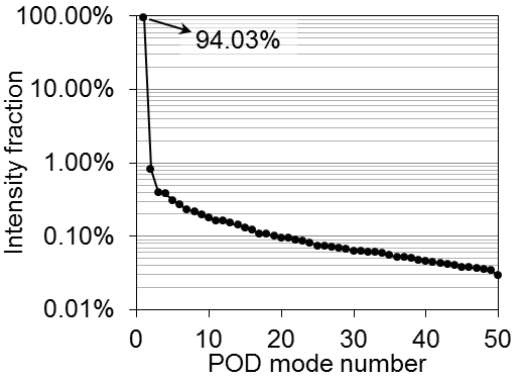

FIG. 10: The captured image intensity fraction for all 50 modes.

that the pattern and its coefficient of mode 1 provide the dominant spray pattern, which resembles the ensemble-averaged image. As depicted in Fig. 11, after mode 2 is added to mode 1, the ensemble-averaged image has been slightly modulated with more spatial variation shown around the center plume. If all 50 mode patterns and their coefficients are used, the resulting image is identical to the original image pattern of cycle 19, as shown in the right image of Fig. 11. This confirms that the higher mode patterns can capture the small-scale spray structures surrounding the edge of the spray. The small-scale structures also represent the well-atomized portions of the spray structure with the ambient gas. These small structures over many cycles can now be compared and quantified. Note that the above features of POD are illustrated only with one instantaneous spray cycle. Other cycles behave in a similar manner, but the modulation degree or well-atomized proportion of finer spray structures may vary more or less from cycle to cycle.

6.4 QUANTIFICATION OF THE CYCLE-TO-CYCLE VARIATIONS OF PULSING SPRAY

In this section, the effects of injection pressure, ambient pressure, and fuel type on the cycle-to-cycle variations of pulsing sprays are presented. The experimental conditions

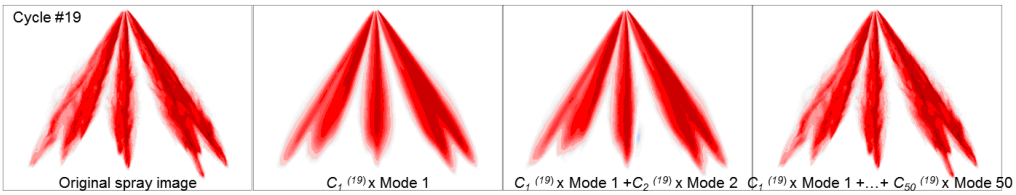

FIG. 11: Original spray image cycle 19, reconstructed spray image cycle 19 using the first mode, first two modes, and all 50 modes ($c_1^{(19)}$ = 687,423, $c_2^{(19)}$ = 91,124, $c_{50}^{(19)}$ = 4,608).

have been discussed in Section 2. Even though the spray variations under the quiescent-ambient air condition are rather small, the subtle variations in different spray cycles can still be clearly demonstrated using POD analysis. Recall from the discussions in Section VI that it is evident that the dominant ensemble-averaged spray pattern of all 50 cycles can be fully captured by the pattern and coefficients of the first mode. High intensity fraction can be found in the first mode provided that the input spray images are highly repeatable. Theoretically, the first mode should capture 100% of intensity if all fifty input spray images are exactly the same. Other higher-mode patterns can differentiate the smaller-scale structures seen along the periphery of the spray boundary.

Figure 12 shows the intensity fraction as a function of POD modes for two injection pressures at 5 and 10 MPa. Two important observations can be found in Fig. 12. First, for both injection pressures, the first mode pattern captures more than 94% of intensity fraction. This suggests that the spray does not vary so much for both injection pressures. The first mode captures about 1% more intensity fraction for 5 MPa than the 10 MPa injection pressure. Second, using the higher modes of POD, it is possible to distinguish the differences of spray variation for two injection pressures even though they are small. It is evident from Fig. 12 that the intensity fractions are slightly less for 5 MPa injection pressure between mode 3 and mode 30. Since higher modes are primarily used for quantifying the finer details along the spray boundary, therefore, by increasing the fuel injection pressure from 5 to 10 MPa, the spray variation slightly increases as a result of the larger portion of well-atomized fuel spray. This is reasonable because sprays are better atomized at higher injection pressure.

Figure 13 shows the intensity fraction as a function of POD modes for the three ambient pressures: 50, 100, and 500 kPa. In the same manner, this figure shows that by increasing the ambient pressure from 50 to 500 kPa, the spray variation increases

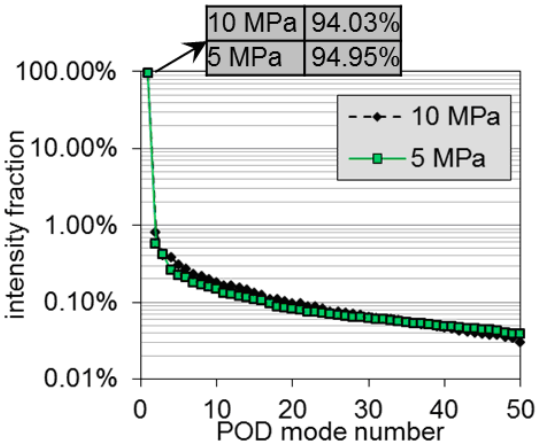

FIG. 12: Intensity fraction captured by POD modes for 5 and 10 MPa injection pressures (n-heptane, 100 kPa ambient pressure, 25°C fuel and ambient temperatures).

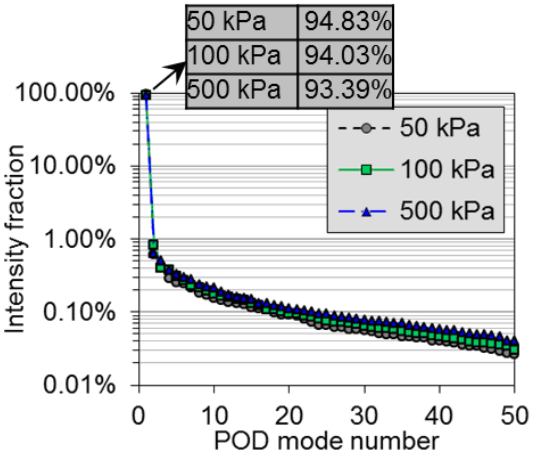

FIG. 13: Intensity fraction captured by POD modes for 50, 100, and 500 kPa ambient pressures (n-heptane, 10 MPa injection pressure, 25°C fuel and ambient temperatures).

slightly. This is possible because as the ambient pressure increases, the increased air density enhances the interaction between the spray and the ambient air (Lefebrve, 1989; Zeng et al., 2012b). Therefore, the spray variation is stronger as the spray becomes better atomized.

Figure 14 depicts the effect of fuel types (n-heptane, ethanol, and gasoline) on the intensity fraction as a function of POD modes. It is evident that the first mode of n-heptane only captures 94.03% of the intensity fraction, which is ∼2% less than the other

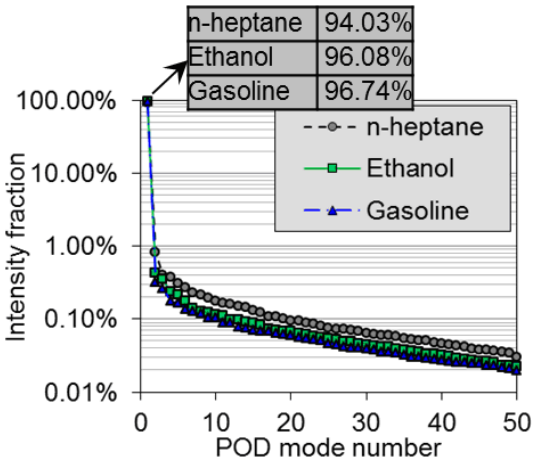

FIG. 14: Intensity fraction captured by the POD modes for n-heptane, ethanol, and gasoline (10 MPa injection pressure, 100 kPa ambient pressure, 25°C fuel and ambient temperatures).

fuels. Therefore, the spray of n-heptane shows slightly larger variation among the three fuels. This is expected, as according to Table 2, the liquid viscosity, liquid density, and surface tension of n-heptane are smallest among the three fuels. Therefore, larger variation and better atomization for n-heptane are expected (Lefebrve, 1989). The physical properties for ethanol and gasoline are similar; therefore, their intensity fraction trends are very close to each other, suggesting that the sprays of these two fuels demonstrate very similar degrees of variation.

7. CONCLUSIONS

In this study, the proper orthogonal decomposition (POD) analysis technique was implemented for the first time to reveal the cycle-to-cycle variation of pulsing spray characteristics. A set of synthetically created scalar fields was employed to demonstrate the basic interpretation of POD modes and coefficients. The POD mode sequence was arranged in a decreasing order in terms of ensemble intensity. Using a set of spray images from a SIDI fuel injector, the physical interpretations of different modes and coefficients of POD on cycle-to-cycle variations of spray characteristics were identified. Specifically, the mode 1 pattern predominantly captured the ensemble-averaged spray pattern, and the coefficients of mode 1 were used to identify the intensity variation among the different cycles of spray. The mode 2 pattern and its coefficients provided the quantification of the spatial variation of the spray plume distribution. Mode 3 and higher modes further identified the cycle variations of the small-scale spray structures, which were typically characterized by the well-atomized portions along the periphery of the fuel spray. Therefore, for a well-atomized fuel spray structure, the higher modes contained a higher proportion of intensity.

Finally, direct visualization of spray structure reveals that a better-atomized spray usually leads to slightly more fluctuations of finer structures along the edges of the spray, which causes higher cycle-to-cycle variations of different pulses. Even though the observation can be visually evident, the results could still be quite subjective, making the quantification of the cycle-to-cycle variation a daunting task. However, as demonstrated in this study, applying POD analysis to multiple cycles of pulsing spray images can quantitatively reveal the subtle differences in spray pattern and intensity variations. Moreover, POD analysis does not require the image to be processed with any user-defined thresholding technique, thus avoiding the subjectivity of an individual's judgment. This study suggests that the POD approach can be used as a novel technique to quantify the cycle-to-cycle variation of pulsing sprays.

ACKNOWLEDGMENTS

This research is sponsored by General Motors R&D Corporation (USA) and National Natural Science Foundation of China (NSFC) under Grants No. 51176115/E060404

and No. 51076093/E060702, and carried out at the National Engineering Laboratory for Automotive Electronic Control Technology of the Shanghai Jiao Tong University. Additional funding support on this research to D. L. S. Hung has also been provided by the 2009 Program for New Century Excellent Talents in University by the Ministry of Education (MOE), China.

REFERENCES

Aleiferis, P. G., Serras-Pereira, J., van Romunde, Z., Caine, J., and Wirth, M., Mechanisms of spray formation and combustion from a multi-hole injector with E85 and gasoline, *Combust. Flame*, vol. **157**, no. 4, pp. 735–756, 2010.

Chen, H., Reuss, D., and Sick, V., Analysis of misfires in a direct injection engine using proper orthogonal decomposition, *Exp. Fluids*, vol. **51**, no. 4, pp. 1139–1151, 2011.

Chen, H., Reuss, D. L., and Sick, V., On the use and interpretation of proper orthogonal decomposition of in-cylinder engine flows, *Measure. Sci. Technol.*, vol. **23**, no. 8, p. 085302, 2012.

Chen, H., Reuss, D. L., Hung, D. L. S., and Sick, V., A Practical guide for using proper orthogonal decomposition in engine research, *Int. J. Engine Res.*, vol. **14**, no. 4, pp. 307–319, 2013.

Cosadia, I., Borée, J., Charnay, G., and Dumont, P., Cyclic variations of the swirling flow in a diesel transparent engine, *Exp. Fluids*, vol. **41**, no. 1, pp. 115–134, 2006.

Druault, P., Guibert, P., and Alizon, F., Use of proper orthogonal decomposition for time interpolation from PIV data, Application to the cycle-to-cycle variation analysis of in-cylinder engine flows, *Exp. Fluids*, vol. **39**, pp. 1009–1023, 2005.

Elbadawy, I., Gaskell, P. H., Lawes, M., and Thompson, H. M., The effect of initial ambient turbulence levels on iso-octane injection sprays, *Atomization Sprays*, vol. **21**, no. 10, pp. 799–817, 2011.

Enaux, B., Granet, V., Vermorel, O., Lacour, C., Thobois, L., Dugué, V., and Poinsot, T., Large eddy simulation of a motored single-cylinder piston engine: numerical strategies and validation, *Flow, Turbulence Combust.*, vol. **86**, pp. 153–177, 2011.

Fogleman, M., Lumley, J., Rempfer, D., and Haworth, D., Application of the proper orthogonal decomposition to datasets of internal combustion engine flows, *J. Turbulence*, vol. **5**, 2004.

Haworth, D. C., Large-eddy simulation of in-cylinder flows, *Oil Gas Sci. Technol.*, vol. **54**, no. 2, pp. 175–185, 1999.

Hung, D. L. S., Chmiel, D. M., and Markle, L. E., Application of an imaging-based diagnostic technique to quantify the fuel spray variations in a direct-injection spark-ignition engine, SAE Technical Paper No. 2003-01-0062, 2003.

Hung, D. L. S. and Zhong, J., Experimental analysis of the start of fuel cycle-to-cycle variations of solenoid-actuated high pressure fuel injectors, SAE Technical Paper No. 2011-01-1882, 2011.

Hung, D. L. S., Zhu, G. G., Winkelman, J. R., Stuecken, T., Schock, H., and Fedewa, A., A high speed flow visualization study of fuel spray pattern effect on mixture formation in a low pressure direct injection gasoline engine, SAE Technical Paper No. 2007-01-1411, 2007.

Kay, P. J., Bowen, P. J., Gold, M., and Sapsford, S. M., Studies of gasoline direct-injection sprays at elevated ambient gas temperatures and pressures, *Atomization Sprays*, vol. **22**, no. 4, pp. 305–331, 2012.

Lefebrve, A. H., *Atomization and Sprays*, Taylor & Francis, New York, 1989.

Marchi, A., Nouri, J., Yan, Y., and Arcoumanis, C., Spray stability of outwards opening pintle injectors for stratified direct injection spark ignition engine operation, *Int. J. Engine Res.*, vol. **11**, no. 6, pp. 413–437, 2010.

Ozdor, N., Dulger, M., and Sher, E., Cyclic variability in spark ignition engines a literature survey, SAE Technical Paper No. 940987, 1994.

Sick, V., High speed imaging in fundamental and applied combustion research, *Proc. Combust. Inst.*, vol. **34**, no. 2, pp. 3509–3530, 2013.

Sick, V., Chen, H., Abraham, P. S., Reuss, D. L., Yang, X., Gopalakrishnan, V., Xu, M., and Kuo,T.-W., Proper-orthogonal decomposition analysis for engine research. Direkteinspritzung im ottomotor, *VIII Forschungsergebnisse und aktueller Entwicklungsstand bei der Benzin-Direkteinspritzung*, Expertverlag, Renningen, Germany, pp. 1–12, 2012.

Sick, V., Drake, M. C., and Fansler, T. D., High-speed imaging for direct-injection gasoline engine research and development, *Exp. Fluids*, vol. **49**, no. 4, pp. 937–947, 2010.

Voisine, M., Thomas, L., Borée, J., and Rey, P., Spatio-temporal structure and cycle to cycle variations of an in-cylinder tumbling flow, *Exp. Fluids*, vol. **50**, no. 5, pp. 1393–1407, 2011.

Zeng, W., Xu, M., Zhang, G., Zhang, Y., and Cleary, D. J., Atomization and vaporization for flash-boiling multi-hole sprays with alcohol fuels, *Fuel*, vol. **95**, pp. 287–297, 2012a.

Zeng, W., Xu, M., Zhang, M., Zhang, Y., and Cleary, D. J., Macroscopic characteristics for direct-injection multi-hole sprays using dimensionless analysis, *Exp. Thermal Fluid Sci.*, vol. **40**, pp. 81–92, 2012b.

Zeng, W., Xu, M., Zhang, Y., and Wang, Z., Laser sheet dropsizing of flash evaporating sprays using simultaneous LIEF/MIE techniques, *Proc. Combust. Inst.*, vol. **34**, no. 1, pp. 1677–1685, 2013.

Zhang, G., Xu, M., Zhang, Y., Zhang, M., and Cleary, D. J., Macroscopic characterization of flash-boiling multi-hole sprays using planar laser induced exciplex fluorescence technique. Part I. On-axis spray structure, *Atomization Sprays*, vol. **22**, no. 10, pp. 861–878, 2012a.

Zhang, M., Xu, M., Zhang, Y., Zhang, G., and Cleary, D. J., Flow-field investigation of multi-hole superheated sprays using high-speed PIV. Part I. Cross-sectional direction, *Atomization Sprays*, vol. **22**, no. 11, pp. 983–995, 2012b.

Zhao, F., Lai, M. C., and Harrington, D. L., Automotive spark-ignited direct-injection gasoline engines, *Progress Energy Combust. Sci.*, vol. **25**, no. 5, pp. 437–562, 1999.

Zhong, J., Hung, D. L. S., Wang, Z., Zhang, Y., and Xu, M., Comparing the cycle-to-cycle variations of pulsing spray characteristics by means of ensemble image and probability presence image analysis techniques, *Proceedings of 12th Triennial International Conference on Liquid Atomization and Spray Systems*, Eva Gutheil and Cam Tropea, Heidelberg, Germany, Sept. 2–6, 2012.